Published in final edited form as:
Neuroimage. 2010 January 1; 49(1): 193–198. doi:10.1016/j.neuroimage.2009.07.017.

On the contribution of deoxy-hemoglobin to MRI gray-white matter phase contrast at high field

Jongho Lee[1], **Yoshiyuki Hirano**[2], **Masaki Fukunaga**[1], **Afonso C. Silva**[2], and **Jeff H. Duyn**[1]

[1]Advanced MRI Section, Laboratory for Functional and Molecular Imaging, National Institute of Neurological Disorders and Stroke, National Institutes of Health, Bethesda, Maryland [2]Cerebral Microcirculation Unit, Laboratory for Functional and Molecular Imaging, National Institute of Neurological Disorders and Stroke, National Institutes of Health, Bethesda, Maryland

Abstract

High field (≥ 7 T) MRI studies based on signal phase have been used to improve visualization of the fine structure of the brain, most notably the major white matter fiber bundles, the gray-white matter subdivision, and the laminar cortical architecture. The observed contrast has been attributed in part to local variations in magnetic susceptibility arising from iron in storage proteins and tissue lipid. Another contribution could come from the paramagnetic blood constituent deoxy-hemoglobin, the tissue concentration of which may vary through local variations in vascular density. To investigate this possibility, we examined phase contrast between gray and white matter in rats after intravenous administration of a superparamagnetic contrast agent at various dosages. At the maximum dosage (3 mg Fe/kg), which resulted in an estimated paramagnetic susceptibility shift 4–8 times larger than deoxy-hemoglobin, we observed a negligible increase in phase contrast between gray and white matter. This result suggests that endogenous deoxy-hemoglobin has no significant contribution to phase contrast between gray and white matter.

Keywords

phase contrast image; deoxy-hemoglobin; high field; USPIO; iron oxide nano-particle

Introduction

Despite the fact that the MR signal provides both amplitude and phase information, the latter is generally discarded in the final steps of the image reconstruction process. Exceptions are in applications such as phase-contrast angiography (Moran, 1982), MR temperature mapping (Ishihara et al., 1995), venography (Reichenbach et al., 1997) and fMRI (Lee et al., 2007; Buracas et al., 2008) in which phase has been demonstrated to provide valuable information.

Recent studies at high magnetic field (≥ 7 T) have indicated that the phase of images acquired with GRE techniques might also provide useful contrast for the study of brain anatomy (Abduljalil et al., 2003; Duyn et al., 2007). For example, in some brain regions, phase provides

Address correspondence to: Jongho Lee, 9000 Rockville Pike, Building 10, Room B1D723A, Bethesda, MD 20892-1065, TEL: (301) 451-9919, FAX: (301) 408-1981, E-MAIL: jonghoyi@mail.nih.gov.

improved contrast-to-noise ratio (relative to magnitude images) for the separation of gray and white matter and has improved visualization of cortical laminar structure (Duyn et al., 2007).

Several sources have been suggested to contribute to the phase contrast in GRE images. A resonance frequency shift and the accompanying image phase accumulation could result from locally altered magnetic susceptibilities originating from compounds such as iron (Ogg et al., 1999; Haacke et al., 2005; Duyn et al., 2007), myelin (Ogg et al., 1999; Duyn et al., 2007), and deoxy-hemoglobin (Haacke et al., 2004). This shift depends on the geometry of the susceptibility distribution and its orientation relative to the main magnetic field (B_o) (Shmueli et al., 2009). Additional phase accumulation might originate from the exchange of water protons with macromolecules that experience resonance frequency shift (Zhong et al., 2008).

However, the relative contribution of each of these sources is not yet well understood. For example, the paramagnetic frequency shift (i.e. a shift to higher frequencies relative to that of pure water) in cortical segments parallel to B_o as observed in Fig. 1 (Duyn et al., 2007;Hammond et al., 2008) can be explained by a higher concentration of paramagnetic iron compound in gray matter, a higher concentration of diamagnetic myelin in white matter (O'Brien and Sampson, 1965), or a higher macromolecular concentration in gray matter (Zhong et al., 2008). Alternatively, significantly larger capillary density in gray matter compared to white matter (Dudley, 1982;Reina-De La Torre et al., 1998; Cavaglia et al., 2001) may also contribute to the paramagnetic phase shift in gray matter due to paramagnetic deoxy-hemoglobin in the capillary bed and intracortical venules. More likely, a combination of multiple of these contrast sources, in addition to other possible contributors, may be responsible for the observed gray and white matter phase contrast. In order to fully understand the origins of phase contrast and to interpret current findings, it is of great interest to investigate the contribution of each of these sources.

One way to investigate the contribution of deoxy-hemoglobin to phase contrast is to vary its concentration. Recently, oxygen challenge studies in humans (Sedlacik et al., 2008) and rodents (Marques et al., 2009) have demonstrated a relatively small or negligible contribution of deoxy-hemoglobin to gray and white matter phase contrast. However, the quantitative results of these two experiments do not agree and the precision of the experiments was limited due to the modest contrast modulation produced by the oxygen challenge (Sedlacik et al., 2008). In addition, blood volume changes associated with the challenge may have affected the results. Therefore, these studies may have not fully eliminated intravascular deoxy-hemoglobin as a potential significant contributor to the gray and white matter phase contrast.

In the present study, we attempted to estimate the contribution of deoxy-hemoglobin to phase contrast between gray and white matter by strongly altering the intravascular susceptibility shift. By administering a paramagnetic intravascular contrast agent to anesthetized rats, we were able to increase the susceptibility shift by an estimate of 8-fold relative to that of deoxy-hemoglobin. This allowed us to precisely estimate the dependence of phase contrast on deoxy-hemoglobin variations related to vascular density differences in cortex (gray matter) and corpus callosum (white matter).

Methods

Paramagnetic susceptibility shifts were induced by intravascular injection of ultrasmall iron oxide particles in solution (USPIO, Molday ION, BioPAL, Worcester, MA, USA). Prior to the *in vivo* experiments in rats, the effect of the contrast agent on magnetic susceptibility was quantified by measuring the induced frequency shifts in cylindrical tubes parallel to B_o. The main purpose of this was to measure the effect size relative to deoxy-hemoglobin. Four tubes (length = 70 mm, and diameter = 5 mm) with various concentrations of USPIO in 0.9% saline

were placed in a large cylindrical container (0.9% saline filled, length = 115 mm, and diameter = 26 mm) also parallel to B_o. The USPIO concentrations were 0 μg Fe/ml, 14.6 μg Fe/ml, 29.2 μg Fe/ml, and 43.7 μg Fe/ml; This corresponded to 0 mg Fe, 1 mg Fe, 2 mg Fe, and 3 mg Fe per kg of rat body weight respectively (assuming blood volume of 68.6 ml per kg of the animal weight (Probst et al., 2006)). A single axial slice through the phantom was scanned using a 2D multi-echo GRE sequence with FOV = 12.8 × 12.8 mm^2, resolution = 100 × 100 μm^2, slice thickness = 2 mm, acquisition bandwidth = ± 26 kHz, flip angle = 60°, TR = 1 sec, and TE = 5 / 10 msec. The frequency was estimated from the phase difference between the two echoes. The background field variation was removed by fitting 8^{th} order polynomials to the outside area of the four cylinders within the phantom.

After these calibration measurements, a 1 mg Fe/ml USPIO solution in 0.9% saline was injected intravenously in five male Sprague-Dawley rats (314 ± 12 g). All animal experiments were performed under the guidance of National Institutes of Health Guide for the Care and Use of Laboratory Animals, and approved by the NINDS/NIDCD Animal Care and Use Committee. The rats were anesthetized with isoflurane (5% induction, 2% maintenance) and a 23 gauge butterfly needle attached to a 50 cm long infusion PE-50 line was inserted to the lateral tail vein to allow contrast agent administration. Before the cannulation of the vein, the total inner volume (typically less than 0.3 ml) of the injection line and the needle was measured using a heparinized saline solution. For one rat, the infusion line was inserted into the femoral vein. Once prepared for the scan, animals were secured to an MRI compatible head holder by means of a tooth bar and ear bars. During the scan, animals were breathing a 7:3 mixture of medical air and oxygen gas containing 2% isoflurane. The rectal temperature was monitored and maintained at 37 °C using an electrical body heater (Rapid Biomedical, GmbH, Rimpar, Germany). Other physiological parameters such as respiration rate, end-tidal CO_2, heart rate and SPO_2, were also monitored throughout the scan.

Three injections, each with 1 mg Fe per kg body weight, were administrated sequentially at 25 minute intervals. MRI scanning was performed prior to injection and four minutes after each injection. The final dosage reached approximately 3 mg Fe/kg since the half-life of the USPIO was much longer (> 10 hr, unpublished result) than the scan time after the first injection (75 min). After each USPIO injection, a predetermined amount of saline (< 0.7 ml) was applied to flush the infusion line and to ensure full delivery of the USPIO solution to the animals.

All scans were performed in a 7 Tesla / 30 cm USR (Bruker BioSpin, Ettlingen, Germany) animal MRI system equipped with a 15 cm gradient set (Resonance Research Inc., Billerica, MA, USA) capable of delivering 450 mT/m within 130 μs rise time. A 12 cm linear home-built birdcage coil was used for excitation, and a four-element phased-array coil (Bruker Biospin, Ettlingen, Germany) was used for signal reception. The scan sequence for the phase images consisted of a 2D multi-echo GRE sequence with the following parameters: FOV = 25.6 × 25.6 mm^2, in-plane resolution = 67 ×67 μm^2, slice thickness = 500 μm, slice gap = 250 μm, acquisition bandwidth = ± 26 kHz, flip angle = 50°, TR = 800 msec, TE = 7 / 16 / 25 msec, number of averages = 4, number of slices = 8 (axial), and total scan time = 20 min. Region of interest based shimming (MAPSHIM, Bruker) was targeted to the brain area under study to minimize large scale B_o inhomogeneity.

The magnitude images were reconstructed from the root sum of squares of the individual coil magnitude images. All images were spatially realigned to the pre-injection images to remove scanner-induced image shifts. Then, a mask was manually selected to separate brain area from surrounding tissues. A slightly tight mask was chosen to reduce the phase variations from pial (surface) veins. After that, the phase images for the mask (i.e. brain) area were reconstructed as follows: first, the individual coil data were complex summed after correcting for the individual coil phase offsets that were calculated from the center voxels of the images (de Zwart

et al., 2002). After coil-combining, phase images within the mask were unwrapped (Jenkinson, 2003) in 3D mode. Large scale phase variations were removed by a 2nd order polynomial fitting in the slice direction and a 2D Gaussian high-pass filter (FWHM = 26 voxels) in the in-plane direction. The frequency images were calculated from the unfiltered phase images using a least-squares estimation weighted by the magnitude image. Then, the background phase variation was removed using the procedure described above. The R_2^* values were also calculated from the magnitude of the multi-echo data.

Results

The USPIO induced frequency shift measured in the phantom amounted to 2.42 Hz/μg Fe/ml (Fig. 2). This corresponds to a 35.3 Hz frequency shift for 1 mg Fe/kg dosage used in the animal experiments. The linear fit for the 14.6 to 43.7 μg Fe/ml dosage data yielded a very high R^2 value (= 0.996). When compared to the blood induced frequency shift in the infinite cylindrical model parallel to the B_o field (Chu et al., 1990;Boxerman et al., 1995), the 43.7 μg Fe/ml (3 mg Fe/kg dosage) causes a 3.9 times larger susceptibility shift (from saline) compared to blood with a fractional hematocrit (Hct) of 0.4, and oxygen saturation level (Y) = 0.7. This assumes a susceptibility difference between pure water and fully deoxygenated blood of 0.18 ppm in CGS units (Weisskoff and Kiihne, 1992). The difference increases to 7.8 times for blood with the values of Hct = 0.3 (Sakai et al., 1985) and Y = 0.8, which more closely resemble the conditions of the capillary bed.

An example of the dose-dependent phase contrast in rats is shown in Fig. 3. Two important observations can be made from this data: First, the large intracortical vessels become more conspicuous with increasing dosages (a–d), suggesting a strong vascular susceptibility shift; Second, there is a substantial contrast between gray (cortex) and white matter (corpus callosum) that appears independent of dosage despite the significantly higher capillary volume in cortex compared to corpus callosum (Cavaglia et al., 2001). This phenomenon is further analyzed in Fig. 4. The subtraction of pre- and post injection data suggests that there is a strong effect in the largest intracortical vessels in the absence of a diffuse gray-white matter effect.

To quantitatively compare the frequency difference between gray and white matter, regions-of-interest (ROI) for cortex and corpus callosum were carefully drawn excluding the cortical surface areas to avoid surface veins (Fig. 3e). These regions were chosen in structures that had substantial extent in the B_o direction, mimicking the situation in published human studies (Abduljalil et al., 2003;Duyn et al., 2007) and ensuring a substantial effect from bulk susceptibility shifts on the image phase. The measured frequency shifts in cortex relative to corpus callosum were 1.08 ± 0.05, 1.27 ± 0.07, 1.46 ± 0.06, 1.59 ± 0.14 at each dosage respectively demonstrating a linear increase with increasing dosages (Fig. 5, dashed line). When the large vessels and surrounding areas were masked out of the ROI (Fig. 3f), the relative frequency shifts reduced to 1.04 ± 0.07, 1.10 ± 0.10, 1.16 ± 0.08, and 1.19 ± 0.10 Hz in each dosage respectively (Fig 5, solid line). Hence, after removing the large vessel effects, the slope of the contrast change decreases significantly. This drop in the slope indicates that most of the contrast increase originates from the larger intracortical vessels, leaving only 0.15 Hz difference between the maximum dosage and pre-injection result for smaller size vessels. Note that a certain portion of this increase might originate from venules that were not identified during the masking procedure due to the limited resolution used in the study. Hence the contrast increase originating from the capillary bed may be even smaller.

Potential regional variations in vascular contrast were investigated by subdividing the original gray and white matter ROIs into three sub-regions. The results of this analysis (Fig. 6) showed similar phase contrast increases with the increasing USPIO dosages in all three sub-ROIs. Note that small differences in the phase contrast in each sub-ROI were observed. These differences

might originate from myelin density and/or iron content variation and possibly from microstructural orientation differences of the fibers. Further research will be required to determine the source of this variation.

To quantify the effect of the contrast agent from the *in vivo* data, the phase shifts in large intracortical veins (on average seven veins in each dataset with mean 116 voxels) relative to white matter (whose frequency shift is relatively close to CSF and water (Duyn et al., 2007)) were measured from the image phase at the first echo (Fig. 7). At the highest dose, the susceptibility in these veins increased by a factor of 3.89 ± 0.56 compared to that of the pre-injection veins. This susceptibility increase matches with the estimation value (3.9) in the phantom experiment when Y = 0.7 and Hct = 0.4. Considering the higher deoxy-hemoglobin content (assuming Y = 0.7) and hematocrit (0.4) of intracortical veins compared to capillary parameters (assuming Y = 0.8 and Hct = 0.3 (Sakai et al., 1985)), the contrast agent induced susceptibility in the capillary bed could reach up to 7.8 times that of the deoxy-hemoglobin induced susceptibility shift (both relative to water). Despite this large increase in intravascular susceptibility, the phase contrast between gray and white matter shows only a 0.15 Hz increase (or 0.51 Hz when including large vessels). This suggests that the maximum contribution of deoxy-hemoglobin, at a 7.8 times lower susceptibility shift, would contribute only 0.02 Hz (or 0.11 Hz when the large vessels portion was adjusted by a factor of 3.9) to gray-white matter contrast. Hence, the contribution of deoxy-hemoglobin is practically negligible relative to the much larger gray-white matter phase contrast of around 1 Hz in rats and up to 5 Hz in humans (Duyn et al., 2007; Hammond et al., 2008).

Discussion and Conclusions

Our results demonstrate both qualitatively and quantitatively that in GRE phase imaging, the contrast between the gray (cortex) and white matter (corpus callosum) in rats is minimally affected by the strong increases in the intravascular susceptibility induced by a USPIO contrast agent. This indicates that much smaller susceptibility shifts caused by deoxy-hemoglobin in the cerebral vasculature do not significantly contribute to the gray-white matter phase contrast. This suggests that the gray-white matter phase shifts encountered in human studies are not due to variations in vascular density, as cortical vascular architecture is similar across mammalian species. Even when effects of the larger intracortical vessels were included, a situation typical for human studies, the estimated frequency shifts due to intravascular deoxyhemoglobin were only a small fraction of the observed gray-white matter frequency shifts.

To further quantify the relative effect of the USPIO used in our study, the R_2^* values were analyzed in individual dosages. The R_2^* in gray matter increased sequentially (23.4 ± 0.7, 30.0 ± 1.4, 37.6 ± 2.4, 44.3 ± 2.6 s^{-1}) with the increasing dosages. These values are much larger than those present during physiologic variations in deoxy-hemoglobin content. For example, based on a 4.3% fMRI signal change measured in layer IV at a 16 msec echo time (Yang et al., 1996), and a baseline R_2^* of 23.4 s^{-1} measured in our experiment, activation induced reductions in deoxy-hemoglobin lead to a R_2^* change (ΔR_2^*) of 2.7 s^{-1}.

This change is 7.7 times smaller than the ΔR_2^* between the pre-contrast data and the highest dosage of our USPIO experiment. Similarly, when the signal change of 5.7% measured at layer IV-V at 11.7 T at 10 msec TE (Silva and Koretsky, 2002) is scaled for 7 T, the ΔR_2^* is estimated to be 2.1 to 3.5 s^{-1} depending on the assumed dependence (linear or quadratic) on field strength. This R_2^* change is also 6 – 10 times smaller than ΔR_2^* change observed in our experiment. Since the R_2^* change has been suggested to linearly correlate with susceptibility change (Thulborn et al., 1982; Yao et al., 2009), the effect of the contrast agent in our experiment is approximately 6 to 10 times larger than what would be observed in fMRI.

In our analysis, the oxygen saturation fraction (Y) for the large intracortical veins was assumed to be 0.7. This value is a midpoint between the Y value (= 0.61) measured in human venous blood (Silvennoinen et al., 2003) and the Y value (= 0.80) measured in rats (Lee et al., 1999). For the capillary bed, Y = 0.8 was used, which is close to 0.77 suggested in (Silvennoinen et al., 2003) but the value must be lower than what it was in the rat experiments (Lee et al., 1999) since the capillary oxygenation saturation level is generally higher than that of the vein. When the capillary oxygenation saturation level is assumed as a mean value of the arterial and venous oxygenation in (Lee et al., 1999), it becomes 0.89. Despite these variations, the upper bound for the deoxy-hemoglobin effect in the gray and white matter phase contrast still remains below 0.03 Hz when the Y value is assumed from the human data or further reduces to 0.01 Hz when the Y values is assumed from the rat data. This upper bound for the deoxy-hemoglobin effect in the gray and white matter phase contrast is much stricter than what has been previously suggested (Duyn et al., 2007; Zhong et al., 2007; Sedlacik et al., 2008). One possible explanation is the complicated structure of the capillary bed cancels out large portions of its own phase shift, resulting in much reduced effects (Menon, 2002).

A previous work by Sedlacik et al. in humans (Sedlacik et al., 2008) showed an increase in the gray and white matter phase contrast with increasing CO_2 concentrations (0.62×10^{-3} rad at 1.67% CO_2, 1.16×10^{-3} rad at 3.33% CO_2, and 1.61×10^{-3} rad at 5.00% CO_2). The phase contrast at 5.00% CO_2 corresponds to 0.03 Hz frequency shift when scaled to 7 T. Since the result was obtained at a larger voxel size ($0.5 \times 0.75 \times 2.0$ mm^2), it agrees with our result that shows a phase contrast increase when large vessels were included. A phase contrast increase with reduced vascular deoxy-hemoglobin content was also observed in an fMRI experiment (Zhao et al., 2007). In this study, the observed phase change by the BOLD fMRI experiment is somewhat larger (0.19 Hz when scaled to 7 T) than expected. A possible explanation for this larger phase contrast is the contribution of surface veins as pointed out in Zhao's paper. On the other hand, a recent study by Marques et al. in rats (Marques et al., 2009) suggested no significant changes in the phase contrast in capillary regions. This result is similar to our results when large vessels were masked out of ROI. Our experiments provide complementary and possibly more accurate findings because of the significantly larger susceptibility modulations induced in the capillary bed as compared to the previous experiments. When measured in humans, the fractional oxygen saturation level (Y) in large veins changed from 0.76 in pure oxygen to 0.9 in 5% CO_2 (Sedlacik et al., 2008). In capillaries where the deoxy-hemoglobin induced gray and white matter phase contrast is expected to originate, the fractional oxygenation saturation change should be even smaller and hematocrit is also smaller than that of veins. Hence, the amount of susceptibility change is limited in these experiments. Moreover, other physiological changes including the blood volume increase could confound the quantitative interpretation of the results. Therefore our data provides further consolidation of the irrelevance of deoxy-hemoglobin as a significant source of the phase contrast between gray and white matter.

The exclusion of deoxy-hemoglobin as a possible source for the gray-white matter phase contrast simplifies the interpretation of phase-based MRI of human brain anatomy. Nevertheless, multiple other potential contributors remain, and the full understanding of the phase contrast will require further research aimed at identifying their relative importance.

Acknowledgment

We thank Xian Feng (Lisa) Zhang for technical assistant with animal preparation.

This research was supported by the Intramural Research Program of the NIH, NINDS.

References

Abduljalil AM, Schmalbrock P, Novak V, Chakeres DW. Enhanced gray and white matter contrast of phase susceptibility-weighted images in ultra-high-field magnetic resonance imaging. J Magn Reson Imaging 2003;18:284–290. [PubMed: 12938122]

Boxerman JL, Hamberg LM, Rosen BR, Weisskoff RM. MR contrast due to intravascular magnetic susceptibility perturbations. Magn Reson Med 1995;34:555–566. [PubMed: 8524024]

Buracas GT, Liu TT, Buxton RB, Frank LR, Wong EC. Imaging periodic currents using alternating balanced steady-state free precession. Magn Reson Med 2008;59:140–148. [PubMed: 18050317]

Cavaglia M, Dombrowski SM, Drazba J, Vasanji A, Bokesch PM, Janigro D. Regional variation in brain capillary density and vascular response to ischemia. Brain Research 2001;910:81–93. [PubMed: 11489257]

Chu SC, Xu Y, Balschi JA, Springer CS Jr. Bulk magnetic susceptibility shifts in NMR studies of compartmentalized samples: use of paramagnetic reagents. Magn Reson Med 1990;13:239–262. [PubMed: 2156125]

de Zwart JA, van Gelderen P, Kellman P, Duyn JH. Application of sensitivity-encoded echo-planar imaging for blood oxygen level-dependent functional brain imaging. Magn Reson Med 2002;48:1011–1020. [PubMed: 12465111]

Dudley, A. Cerebrospinal blood vessels normal and diseased. In: Haymaker, W.; Adams, RD., editors. Histology and histopathology of the nervous system. Charles C Thomas; 1982. p. 714-797.

Duyn JH, van Gelderen P, Li TQ, de Zwart JA, Koretsky AP, Fukunaga M. High-field MRI of brain cortical substructure based on signal phase. Proc Natl Acad Sci U S A 2007;104:11796–11801. [PubMed: 17586684]

Haacke EM, Cheng NYC, House MJ, Liu Q, Neelavalli J, Ogg RJ, Khan A, Ayaz M, Kirsch W, Obenaus A. Imaging iron stores in the brain using magnetic resonance imaging. Magn Reson Imaging 2005;23:1–25. [PubMed: 15733784]

Haacke EM, Xu Y, Cheng YC, Reichenbach JR. Susceptibility weighted imaging (SWI). Magn Reson Med 2004;52:612–618. [PubMed: 15334582]

Hammond KE, Lupo JM, Xu D, Metcalf M, Kelley DAC, Pelletier D, Chang SM, Mukherjee P, Vigneron DB, Nelson SJ. Development of a robust method for generating 7.0 T multichannel phase images of the brain with application to normal volunteers and patients with neurological diseases. Neuroimage 2008;39:1682–1692. [PubMed: 18096412]

Ishihara Y, Calderon A, Watanabe H, Okamoto K, Suzuki Y, Kuroda K, Suzuki Y. A precise and fast temperature mapping using water proton chemical shift. Magn Reson Med 1995;34:814–823. [PubMed: 8598808]

Jenkinson M. Fast, automated, N-dimensional phase-unwrapping algorithm. Magn Reson Med 2003;49:193–197. [PubMed: 12509838]

Lee J, Shahram M, Schwartzman A, Pauly JM. Complex data analysis in high-resolution SSFP fMRI. Magn Reson Med 2007;57:905–917. [PubMed: 17457883]

Lee SP, Silva AC, Ugurbil K, Kim SG. Diffusion-weighted spin-echo fMRI at 9. 4 T: Microvascular/tissue contribution to BOLD signal changes. Magn Reson Med 1999;42:919–928. [PubMed: 10542351]

Marques JP, Maddage R, Mlynarik V, Gruetter R. On the origin of the MR image phase contrast: An in vivo MR microscopy study of the rat brain at 14.1 T. Neuroimage 2009;46:345–352. [PubMed: 19254768]

Menon RS. Postacquisition suppression of large-vessel BOLD signals in high-resolution fMRI. Magn Reson Med 2002;47:1–9. [PubMed: 11754436]

Moran PR. A flow velocity zeugmatographic interlace for NMR imaging in humans. Magn Reson Imaging 1982;1:197–203. [PubMed: 6927206]

O'Brien JS, Sampson EL. Fatty acid and fatty aldehyde composition of the major brain lipids in normal human gray matter, white matter, and myelin. J Lipid Res 1965;6:545–551. [PubMed: 5865383]

Ogg RJ, Langston JW, Haacke EM, Steen RG, Taylor JS. The correlation between phase shifts in gradient-echo MR images and regional brain iron concentration. Magn Reson Imaging 1999;17:1141–1148. [PubMed: 10499676]

Probst RJ, Lim JM, Bird DN, Pole GL, Sato AK, Claybaugh JR. Gender differences in the blood volume of conscious Sprague-Dawley rats. J Am Assoc Lab Anim Sci 2006;45:49–52. [PubMed: 16542044]

Reichenbach JR, Venkatesan R, Schillinger DJ, Kido DK, Haacke EM. Small vessels in the human brain: MR venography with deoxyhemoglobin as an intrinsic contrast agent. Radiology 1997;204:272–277. [PubMed: 9205259]

Reina-De La Torre F, Rodriguez-Baeza A, Sahuquillo-Barris J. Morphological characteristics and distribution pattern of the arterial vessels in human cerebral cortex: a scanning electron microscope study. Anat Rec 1998;251:87–96. [PubMed: 9605225]

Sakai F, Nakazawa K, Tazaki Y, Ishii K, Hino H, Igarashi H, Kanda T. Regional cerebral blood volume and hematocrit measured in normal human volunteers by single-photon emission computed tomography. J Cereb Blood Flow Metab 1985;5:207–213. [PubMed: 3921557]

Sedlacik J, Kutschbach C, Rauscher A, Deistung A, Reichenbach JR. Investigation of the influence of carbon dioxide concentrations on cerebral physiology by susceptibility-weighted magnetic resonance imaging (SWI). Neuroimage 2008;43:36–43. [PubMed: 18678260]

Shmueli K, van Gelderen P, Yao B, de Zwart JA, Fukunaga M, Duyn JH. The dependence of tissue phase contrast on orientation can be overcome by quantitative susceptibility mapping. Proceedings of the 17th Annual Meeting of ISMRM, Honolulu, Hawaii, 2009:466.

Silva AC, Koretsky AP. Laminar specificity of functional MRI onset times during somatosensory stimulation in rat. Proc Natl Acad Sci U S A 2002;99:15182–15187. [PubMed: 12407177]

Silvennoinen MJ, Clingman CS, Golay X, Kauppinen RA, van Zijl PCM. Comparison of the dependence of blood R2 and R2* on oxygen saturation at 1.5 and 4.7 Tesla. Magn Reson Med 2003;49:47–60. [PubMed: 12509819]

Thulborn KR, Waterton JC, Matthews PM, Radda GK. Oxygenation dependence of the transverse relaxation time of water protons in whole blood at high field. Biochim Biophys Acta 1982;714:265–270. [PubMed: 6275909]

Weisskoff RM, Kiihne S. MRI susceptometry: image-based measurement of absolute susceptibility of MR contrast agents and human blood. Magn Reson Med 1992;24:375–383. [PubMed: 1569876]

Yang X, Hyder F, Shulman RG. Activation of single whisker barrel in rat brain localized by functional magnetic resonance imaging. PNAS 1996:475–478. [PubMed: 8552664]

Yao B, Li TQ, Gelderen PV, Shmueli K, de Zwart JA, Duyn JH. Susceptibility contrast in high field MRI of human brain as a function of tissue iron content. Neuroimage 2009;44:1259–1266. [PubMed: 19027861]

Zhao F, Jin T, Wang P, Hu X, Kim SG. Sources of phase changes in BOLD and CBV-weighted fMRI. Magn Reson Med 2007;57:520–527. [PubMed: 17326174]

Zhong, K.; Leupold, J.; Stadler, J.; Tempelmann, C.; Speck, O. A multiple field study of permeability difference between gray and white matters; Proceedings of the 15th Annual Meeting of ISMRM; Berlin, Germany. 2007. p. 205

Zhong K, Leupold J, von Elverfeldt D, Speck O. The molecular basis for gray and white matter contrast in phase imaging. Neuroimage 2008;40:1561–1566. [PubMed: 18353683]

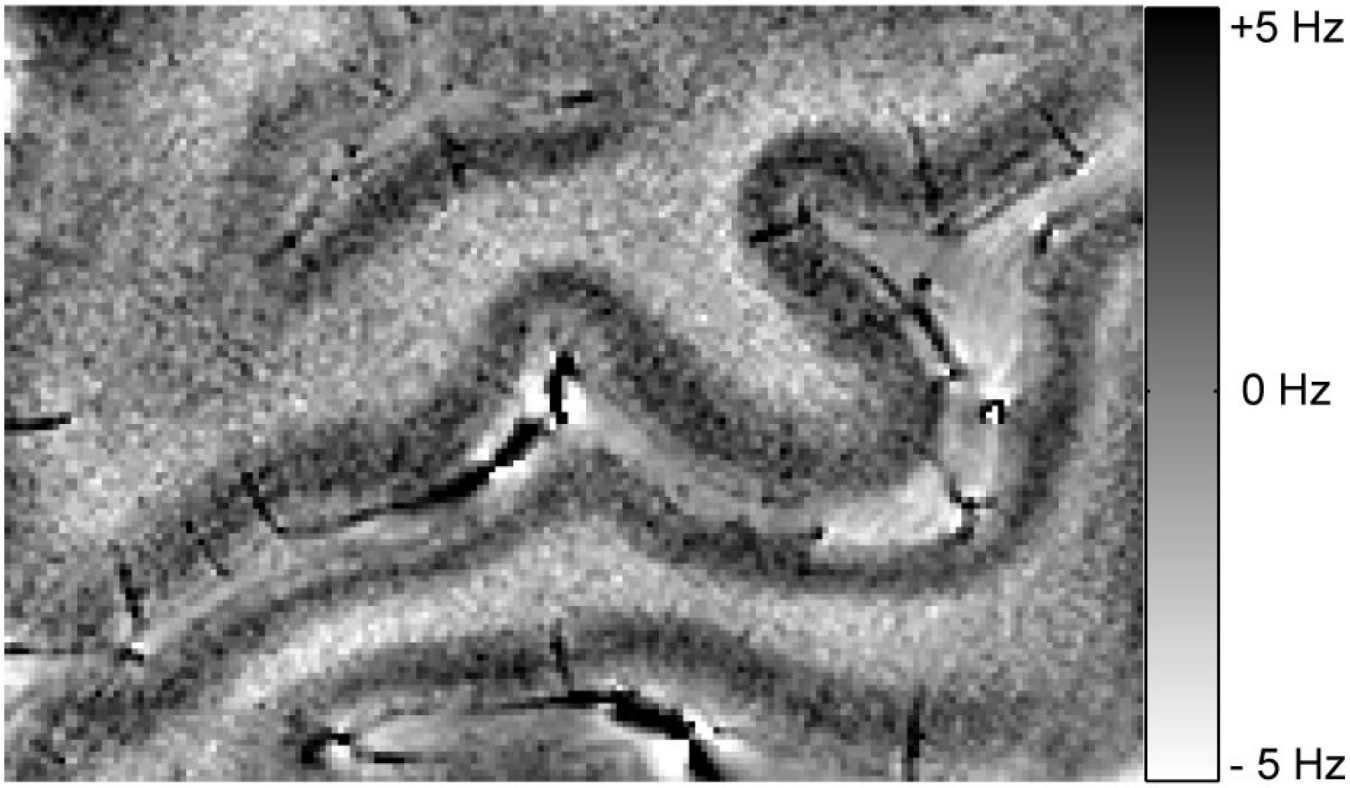

Figure 1.
Example of gray-white matter phase shift observed *in vivo* at 7 T around human central sulcus (in-plane resolution = 0.22 × 0.22 mm^2). A paramagnetic frequency shift of approximately 5 Hz is observed in motor cortex.

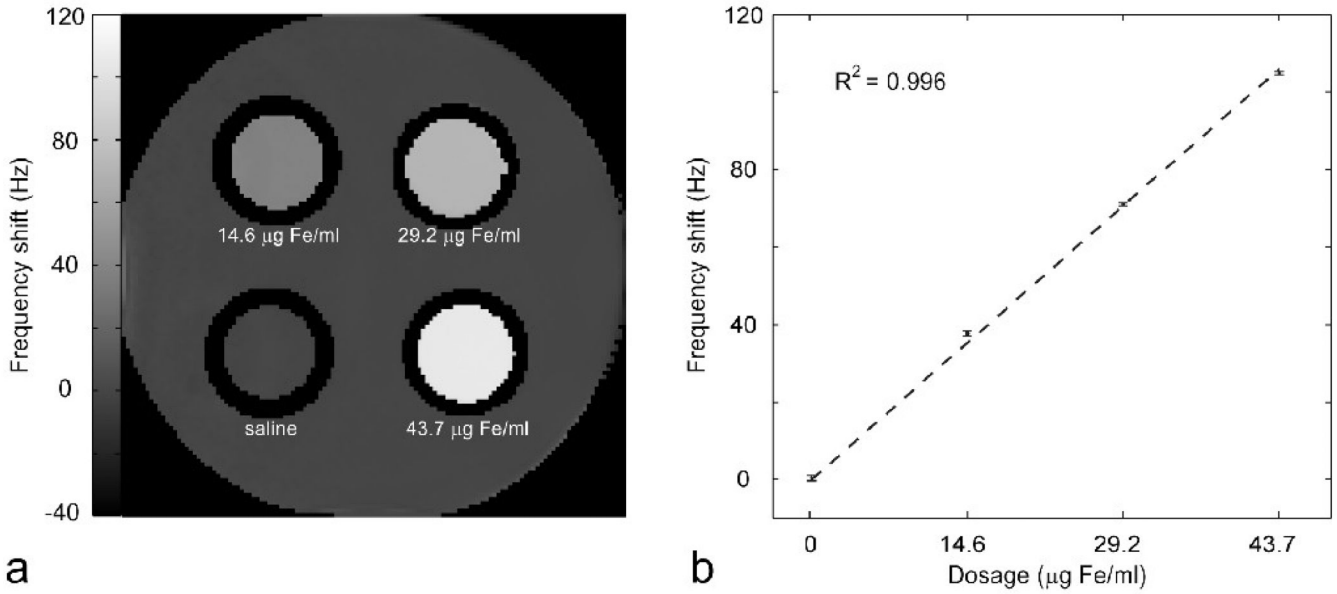

Figure 2.

(a) The phantom with the four different dosages (0 to 43. 7 μg Fe/ml) of USPIO. (b) The frequency shift measured relative to surrounding saline. Note that 1 mg Fe per kg of body weight corresponds to 14.6 μg Fe/ml assuming the 68.6 ml of blood volume per kg of the body weight.

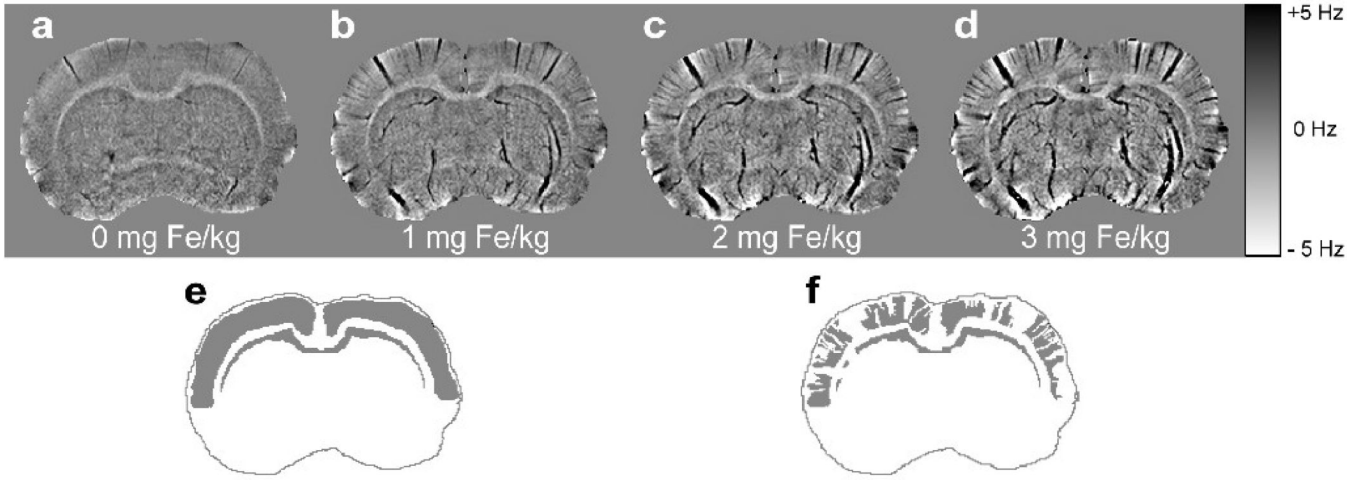

Figure 3.
(a–d) The estimated frequency images at the four different dosages (0 to 3 mg Fe/kg) of the same slice. With increasing dosages, the contrast becomes more prominent near the large intracortical vessels. However, the gray and white matter contrast remains similar. (e) The regions of interest (ROI) without vessel masking. (f) The ROI after vessel masking.

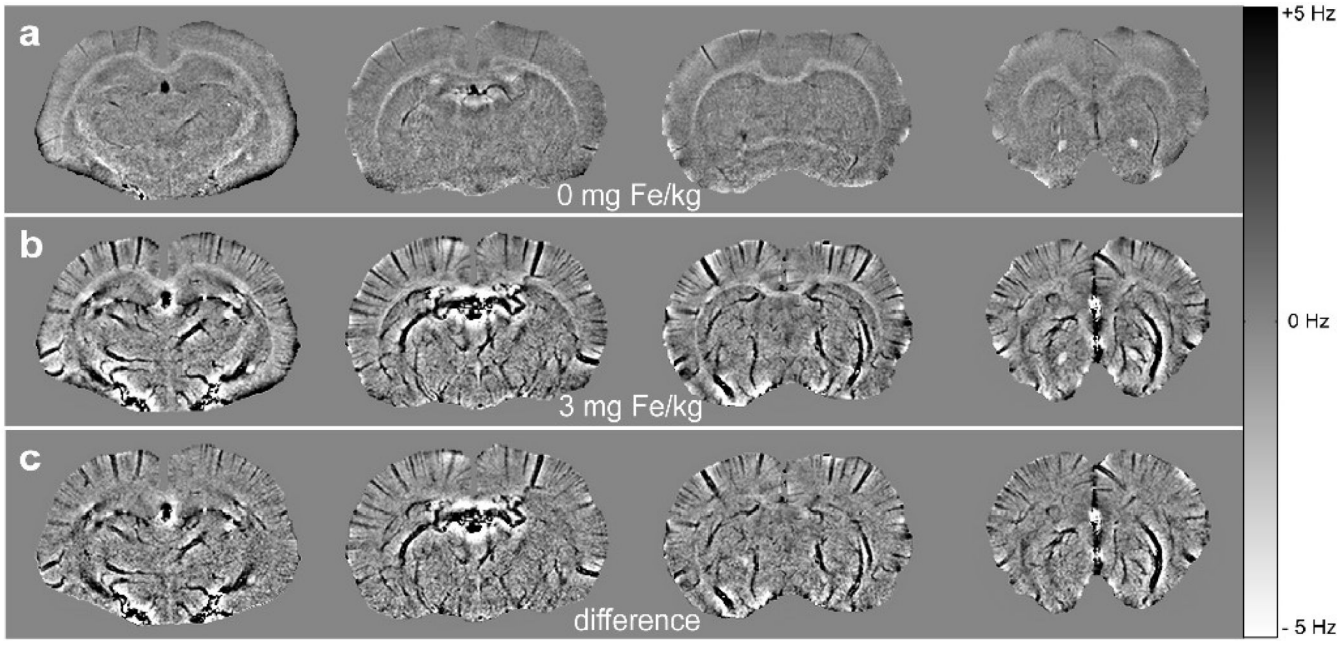

Figure 4.
(a) Pre-injection frequency images (b) 3 mg Fe/kg dosage frequency images, and (c) their difference images (3 mg Fe/kg dosage results minus pre-injection results) at four different slices. There is almost no hint of the gray and white matter contrast in the difference images.

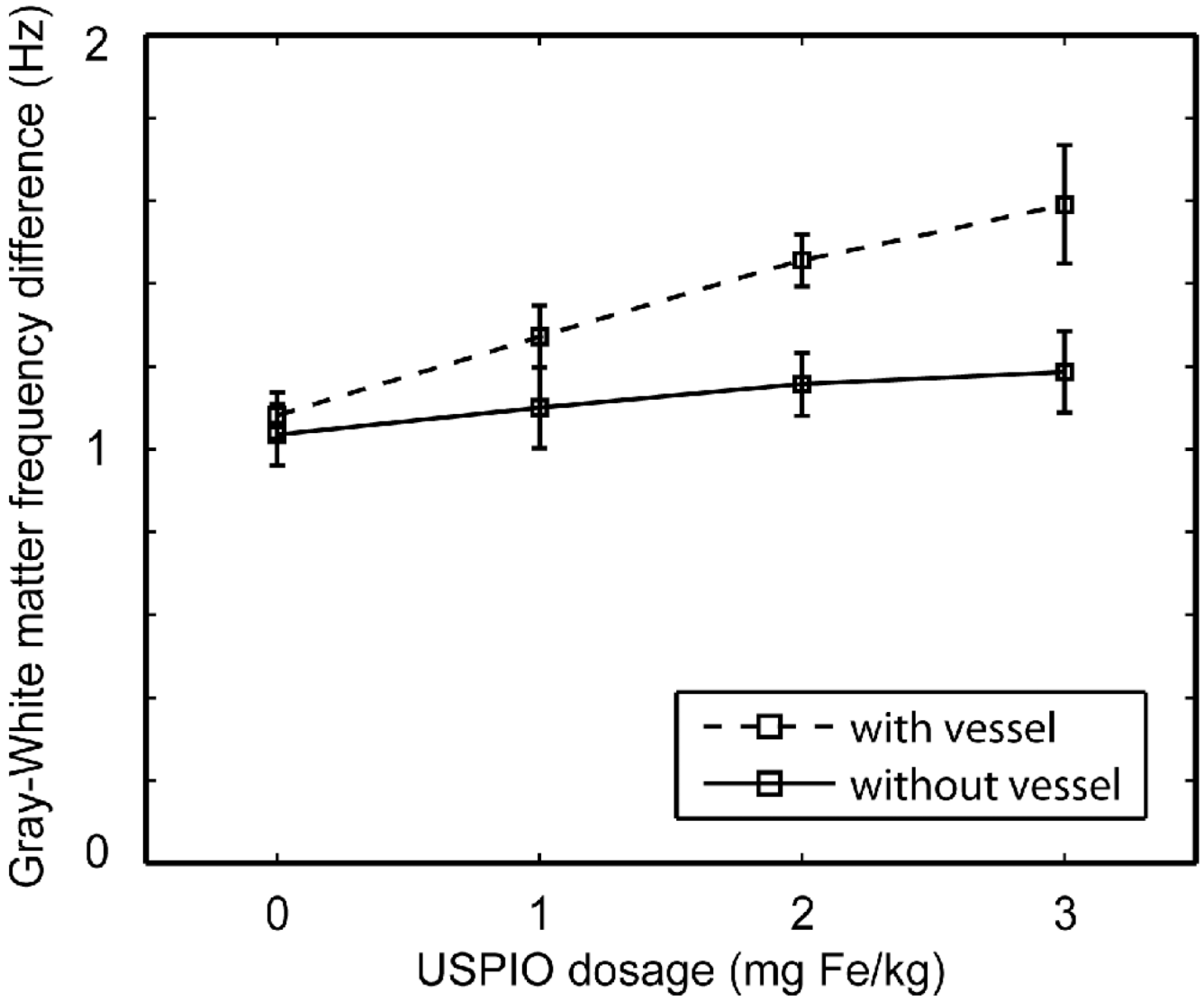

Figure 5.
The gray and white matter phase contrast measured in ROI: including vessels (dashed line) vs. after masking out vessels and surrounding areas (solid line). The slope of the phase contrast change over the four dosages reduces significantly after masking out the vessel areas. The error bars indicate ± 1 standard deviation.

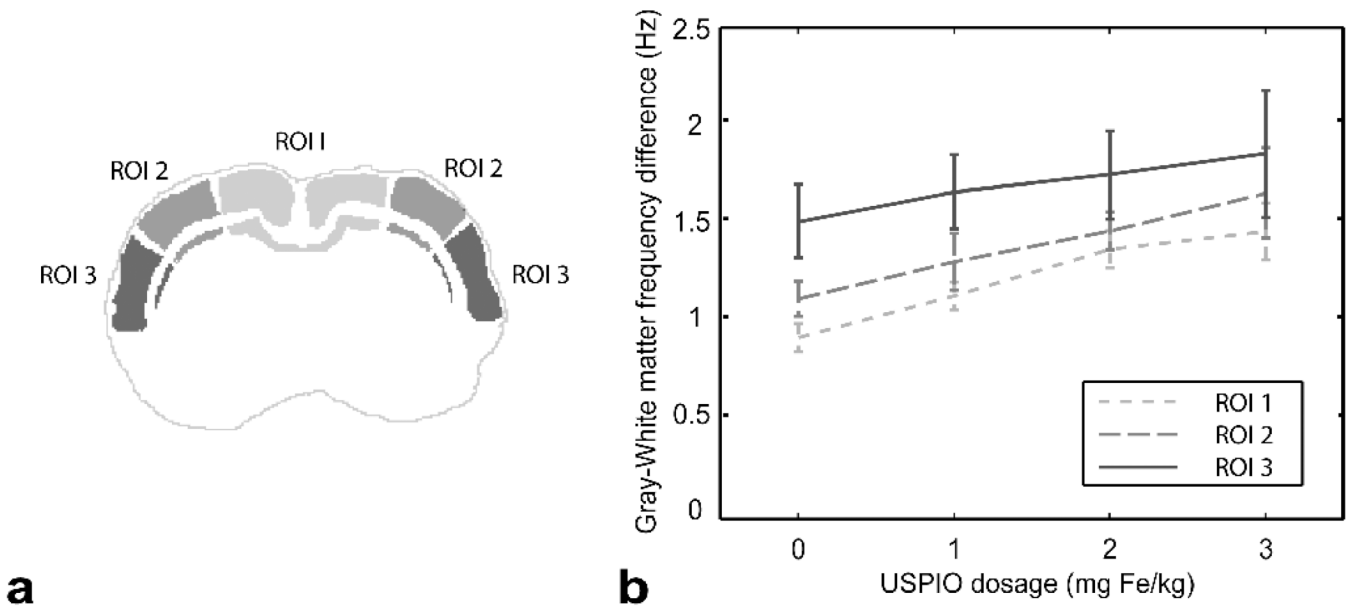

Figure 6.
The sub-regional analysis of the gray and white matter phase contrast. (a) The location of the sub-ROIs. (b) The gray and white matter frequency difference in each sub-region as a function of the contrast dose.

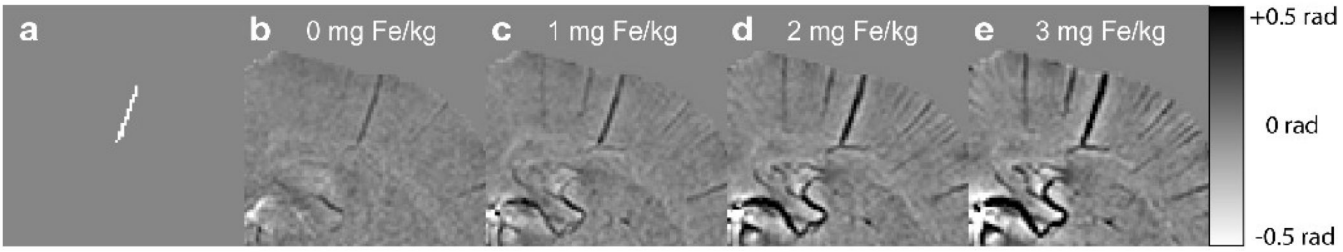

Figure 7.

(a) An example of a large vein location and (b–e) the first echo phase images in each dosage. Note that only large intracortical veins that were easily identified at the first echo phase images of the pre-injection data were chosen. The first echo phase (echo time = 7 msec) were used to avoid any signal drop at higher dosages at later echoes.